Continuous gravity measurement with a portable atom gravimeter

Chen-Yang Li,[1,2,3] Jin-Bao Long,[1,2] Ming-Qi Huang,[1,2,3] Bin Chen,[1,2] Yu-Meng Yang,[1,2,3] Xiao Jiang,[1,2,3] Chuan-Fang Xiang,[4] Zhao-Li Ma,[4] De-Qiang He,[4] Luo-Kan Chen,[1,2,3,*] and Shuai Chen[1,2,3,†]

[1]*Hefei National Research Center for Physical Sciences at the Microscale and School of Physical Sciences, University of Science and Technology of China, Hefei 230026, China*

[2]*Shanghai Research Center for Quantum Science and CAS Center for Excellence in Quantum Information and Quantum Physics, University of Science and Technology of China, Shanghai 201315, China*

[3]*Hefei National Laboratory, University of Science and Technology of China, Hefei 230088, China*

[4]*Zhaotong Earthquake Prevention and Disaster Reduction Administration, Zhaotong, Yunnan 657000, China*

(Received 31 March 2023; revised 27 July 2023; accepted 22 August 2023; published 11 September 2023)

We report here a portable and robust home-built atom gravimeter (USTC-AG11) continuously working in a seismic station in Zhaotong, Yunnan, for over five months. Based on the principle of matter-wave interference, the atom gravimeter is very sensitive to the local gravity and reaches the precision of micro-Gal ($1 \times 10^{-8}\mathrm{m/s^2}$) level. With the technique of vibrational compensation, the sensitivity of the atom gravimeter reaches $38\,\mu\mathrm{Gal}/\sqrt{\mathrm{Hz}}$, the overall noise level is suppressed by 80% compared to the no-vibration-compensation method, and 95% of the vibration noise is effectively suppressed. The design of the atom gravimeter in the electronics and laser optics, especially the laser frequency and phase auto-relock technology, guarantees long-term continuous running. The long-term precision of the atom gravimeters is better than 2 μGal, which is comparable to the best classical gravimeter FG-5(X). Our work provides an application for the high-precision atomic gravimeter based on modern quantum sensing technology in the field of geophysics and geodesy survey.

DOI: 10.1103/PhysRevA.108.032811

I. INTRODUCTION

Since the pioneering work started by Mark Kasevich and Steve Chu in 1991 [1], atom interferometry has accessed to long-term development and grown into a successful tool for precision measurements. Presently, atoms interferometer has been extensively used in fields such as measurements of gravity acceleration [2–7], gradiometry [8–10], rotation [11–14], and tests of fundamental physical laws [15–22]. The atom gravimeter (AG), one of the most significant embranchments of the atom interferometer, has attracted much attention as a result of its existing performance and potential [23] since the precise gravity measurement is valuable in broad areas such as geophysics, geodesy, and aided inertial navigation based on the gravity reference map. At present, the research interests of atom gravimeters are not only limited to scientific research but also include more and more application fields. Portable atom gravimeters are developed towards field applications, which has become a research priority [24,25].

Through development over two decades, the sensitivity and accuracy of atom gravimeters have reached the level of several μGal ($1\,\mu\mathrm{Gal} = 10^{-8}\,\mathrm{m/s^2}$), which is comparable with a high-precision commercial classical gravimeter such as FG-5(X) and A10. In ICAG-2017, six atom gravimeters took part in the comparison, and four of their results are recorded in the official report [26]. Recently, a commercial atom gravimeter AQG-B from μQuants was successfully installed on the Mount Etna volcano and used to observe the variation of the gravity caused by the underground dynamics [27]. Not only for static gravity measurements, the atom gravimeters are also applied in different moving platforms. Müller's group from the University of California performed a field gravity survey along a route of about 7.6 km in Berkeley Hills using a mobile atom gravimeter [28]; Huazhong University of Science and Technology (HUST) reported a car-based portable atom gravimeter that revealed the density distribution of a hill located on HUST campus [29]; Zhejiang University of Technology (ZJUT) also performed a gravity survey with their atom gravimeter around the Xianlin reservoir in Hangzhou City [30]. The French aerospace laboratory ONERA developed a marine atom gravimeter and implemented it in real sea conditions with a measurement accuracy better than 1 mGal [31], and they also loaded it on an airplane to perform the gravity survey in Iceland [32]; ZJUT and Innovation Academy for Precision Measurement Science and Technology, Chinese Academy of Science, also reported their ship-borne atom gravimeter [33,34].

Compared to the classical gravimeter, the atom gravimeter uses laser-cooled atoms as the test mass. It does not have any mechanical movement, therefore mechanical wear has been avoided completely, and this unique attribute brings AG excellent long-term uninterrupted output performance. In this paper, aiming towards the precision gravity measurements for seismic stations, we report a portable and compact atom gravimeter named USTC-AG11 based on matter wave interferometry. We transported the AG over 2200 km from

*lkchen@ustc.edu.cn
†shuai@ustc.edu.cn

Shanghai to Zhaotong, Yunnan Province, deployed the AG in a local seismic station, and carried out a long-term survey over five months. The sensitivity, long-term stability, and overall accuracy of USTC-AG11, respectively, are 38 μGal/$\sqrt{\text{Hz}}$, better than 1 μGal, and about 2 μGal, which is the same level as the best classical gravimeter FG-5(X). Our result implies that the atom gravimeter is an ideal instrument for long-term precise measurements of gravity acceleration g in the near future.

II. SETUP OF THE ATOM GRAVIMETER

The assembly of the USTC-AG11 atom gravimeter consists of three parts: a miniaturized sensor head, a compact laser package, and an electrical control system.

The miniaturized sensor head has a dimension of only 30 cm × 30 cm × 65 cm. The vacuum chamber is made of nonmagnetic metal titanium with a 10^{-9} mbar level vacuum degree. Meanwhile, strong remanence leads to high-order Zeeman effect in the process of atomic matter wave interference, which causes systematic error. We added a double-sheet μ-metal magnetic shield shell to the sensor head to avoid a spray magnetic field with a residual magnetic field below 1 mGauss. There are three regions in the sensor head: the atom preparation region, the matter wave interferometry region, and the quantum state detection region, as shown in Fig. 1(a). In the atom preparation region, a pair of anti-Helmholtz coils are wound on the outer wall of the vacuum chamber to supply magnetic field gradient (10 Gauss/cm) for atom trapping; In the matter waves interferometry region, a pair of Helmholtz coils are wrapped around the outer wall of the vacuum chamber to generate a quantum axis with a uniform magnetic field (∼330 mGauss) for atom interferometry. In the quantum state detection region, a pair of photoelectric diodes are symmetrically mounted on both sides of the vacuum chamber for detecting the atomic quantum state population and improving the detection efficiency (∼12.7%).

A compact laser package has been designed for providing all laser beams to manipulate the quantum states of the ^{87}Rb atom. All laser beams are supplied via two diode lasers (TOPTICA DL-Pro) and a tapered amplifier (TA). One of the diode lasers is locked with a magnetic-enhanced modulated-transfer spectral (ME-MTS) [35], which supplies the repumper beam and Raman master beam. The other one is phase locked using an optical-phase lock loop (OPLL) and amplified by TA, which generates the cooling beams, probe beams, Raman slave beam, and blow-away beam. A laser frequency auto-relocked scheme is designed to ensure that the AG can work without long time intervals. The lasers and optics are all integrated into a 46 cm × 42 cm × 15 cm solid module to achieve mechanical stability and compactness.

The electrical control system chassis for the laser controller, time or clock controller, as well as data acquisition modules [includes atomic fluorescence and ground three-dimensional (3D) vibrational signal] are all integrated into three standard 3U 19 in. electronic boxes and mounted together with the optics module in a 56 cm × 68 cm × 72 cm rack. The total power consumption is less than 250 W.

The working sequence and the main operating parameters of this AG sensor are described as follows: ^{87}Rb atoms as the test mass are loaded directly from the background vapor by the 3D MOT in 120 ms with about 10^8 atoms; After 2 ms of a far-detuned optical molasses, the atoms are further cooled to 3 μK, then we turn off the repumper laser to depump atoms to the $|F = 1\rangle$ state within 1 ms. At the moment, the remaining atomic number is about 10^7; the initial state is prepared through Raman π pulses with a pulse time of about 20 μs interacted with atoms two times, and about 10^6 atoms are selected with a temperature of 200 nK in the vertical direction and populated in the magnetic-insensitive state $|F = 1, m_F = 0\rangle$. To avoid disturbing the atoms populated in the magnetic-sensitive state, the repumper beam as the blowing laser beam is applied to remove the atoms populated in $|F = 1\rangle$ after the first Raman π pulse and a blowing laser beam is introduced

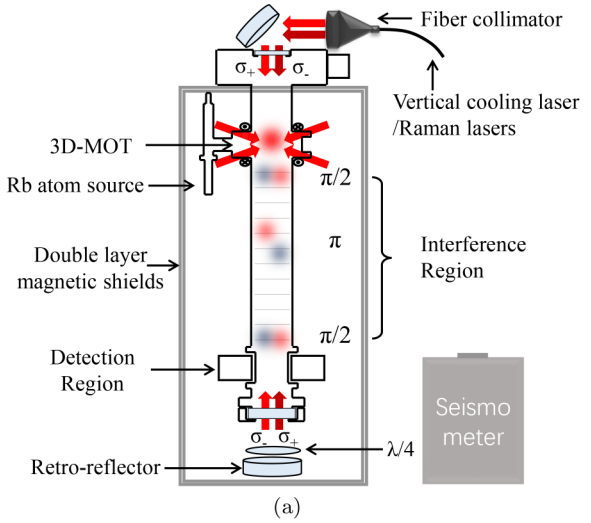

(a)

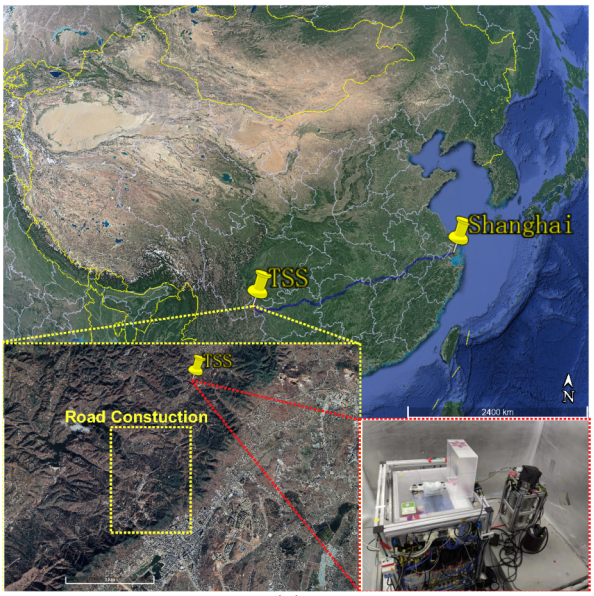

(b)

FIG. 1. (a) Schematic of the sensor head, which presents the basic structure of the sensor head. (b) The location of USTC-AG11 on a satellite map; insert is the real field gravity measurement of USTC-AG11 in TSS

to remove the atoms populated in $|F=2\rangle$ after the second Raman π pulse. All the above processes are finished in the atom preparation region of the sensor head. Mach-Zehnder type matter wave interferometry is realized by deploying a $\frac{\pi}{2}-\pi-\frac{\pi}{2}$ Raman pulse sequence with interaction time $T=82$ ms. To prevent the incoherent single-photon scattering, the Raman lasers have a large red detuning $\Delta \simeq 650$ MHz between the $|F=1\rangle \rightarrow |F'=1\rangle$ transition line. Meanwhile, during the initial state preparation and the interferometry, a uniform magnetic field vertically directed (∼330 mGauss) determines the quantized axis for the atoms located on the interference region. The Doppler frequency shift caused by free falling is compensated by chirping the slave Raman laser frequency at the rate of $\alpha \simeq 25.103$ MHz/s in the interference region. With atoms free-falling into the detection region, two-layer probe beams are introduced to detect the atoms populated in $|F=2\rangle$ and $|F=1\rangle$ quantum states, respectively. The whole working process lasts approximately 0.31 s, which induces a 3.2 Hz repetition rate.

III. PERFORMANCE OF AG IN A FIELD SEISMIC STATION

Analysis of the long-term gravity anomaly provides an efficient method to help identify an incoming earthquake. Since AG can perform a continuous drift-free absolute gravity measurement, it may pave a new way to reveal a continuous record of gravity anomaly. To verify this, we move USTC-AG11 to the Tianhetai seismic station (TSS) located at Ludian, Zhaotong, Yunnan Province. The geography of TSS is 27.25° North, 103.55° East, and 1969 m above sea level. A 66-m-deep tunnel is dug into the mountain, among which we choose a separate room to carry out the long-term gravity survey. Figure 1(b) shows the location of our AG on a satellite map. The inset of Fig. 1(b) shows the real field gravity measurement, the left (right) part of which is the compact laser package and the electronics carbine (the miniaturized sensor head and the highly sensitive seismometer Güralp 3ESPC).

In fact, except for the phase of the gravimeter, various noise is always accompanied by the measurement, especially the vibration phase noise $\phi_{\rm vib}$, hence a vibration noise suppression method is necessary. During the measurement of gravitational acceleration g, we utilize a highly sensitive seismometer Güralp-3ESPC to record the vibration data and calculate the phase shift $\phi_{\rm vib}$ caused by the fluctuation of the Raman reflector. This phase shift is given by [36–38]

$$\begin{aligned}\phi_{\rm vib} &= k_{\rm eff}(z_{\rm g}(0)-2z_{\rm g}(T)+z_{\rm g}(2T))\\ &= k_{\rm eff}\int_0^{2T} g_{\rm s}(t)v_{\rm g}(t)dt\\ &= k_{\rm eff}K_{\rm s}\int_0^{2T} g_{\rm s}(t)U_{\rm s}(t)dt,\end{aligned} \tag{1}$$

where T, $k_{\rm eff}$, $z_{\rm g}$ ($v_{\rm g}$), $U_s(t)$, and $K_s = 2000\,{\rm v/(m/s)}$ are, respectively, interaction time between each Raman pulse, effective Raman wave vector, the position (velocity) of the Raman reflector of the sensor head, the output voltage of the seismometer, and the conversion factor of this seismometer, and the sensitive function $g_s(t)$ can be expressed as

$$g_{\rm s}(t) = \begin{cases} -1 & 0 < t < T, \\ 1 & T < t < 2T. \end{cases} \tag{2}$$

During this measurement, we only chirp three different α points, and the atoms drop three times in one direction for each α point. Simultaneously, we flip the sign of $\vec{k}_{\rm eff}$ to reduce the independent systematic errors of $\vec{k}_{\rm eff}$. Thus, a total of 18 drops are finished within 6 s. Meanwhile, we take an efficient postcorrection method of vibration noise to improve the sensitivity of AG. To demonstrate the validity of this vibrational postcorrection method, we picked out a solid tide match from a whole day, September 25, 2020, to calculate the sensitivity before and after vibration noise postcorrection. As shown in Fig. 2, the black dot is the measured g data by USTC-AG11, the red line is the earth solid tide model, which is calculated by TSOFT software, a commercial tool to calculate the earth tide model. Figure 2(a) shows the solid tide match and the residuals obtained by subtracting the tide model from measured g values. During this day, we can clearly see the difference before and after vibration correction, especially at the working time such as from 9:00 a.m. to 12:00 p.m. and 2:00 p.m. to 6:00 p.m. In the daytime, there was a noticeable increase in noise, which was caused by the construction of an expressway a few kilometers away from TSS at the time, which was the major source of the vibration noise.

To further explain the vibration correction method of our AG during this gravity measurement, we calculate the correlation factor between the phase shift caused by vibration noise and the population probability of atoms, as shown in Fig. 2(b). Different types of noise will cause atomic population fluctuation, and the square of correlation factor represents the contribution of vibration noise to the overall noise. The correlation factor is obtained by calculating the covariance of the vibration phase shift $\phi_{\rm vib}$ and the population $P_{|F=1\rangle}$ of the atoms. In our case, the 0.92^2 means the vibration noise proportion to the overall noise, because the different noises are independent of each other, hence $\sqrt{0.92^2 + C^2_{\rm other\_noise}} = 1$.

To evaluate the noise level of our AG, the sensitivity of our AG is calculated using the standard Allan deviation, which is shown in Fig. 2(c). With vibration correction, the sensitivity has been improved significantly from 84 μGal/$\sqrt{\rm Hz}$ to 38 μGal/$\sqrt{\rm Hz}$. The contribution of the remaining noise is $(38\,\mu{\rm Gal}/\sqrt{\rm Hz})^2/(84\,\mu{\rm Gal}/\sqrt{\rm Hz})^2 \simeq 0.2$, which means that 80% of the overall noise has been suppressed, and the suppressed 80% noise is almost all from the vibration noise, so $0.8/0.92^2 \simeq 0.95$ is suppressed on vibration noise. At the same time, the stability can reach 1 μGal in 1200 s with vibration correction. Thus, this method of suppressing vibration noise is very efficient for stability and long-term measurements of our atom gravimeter.

To verify the long-term stable working ability of our AG, after a short setup time in TSS, the atom gravimeter USTC-AG11 performs a continuous running from July 1 to December 9, 2020, under an unattended mode. Figure 3 shows the continuous solid tide observation of the TSS site over five months. The black points are the gravity values measured by USTC-AG11, and each black point is averaged by

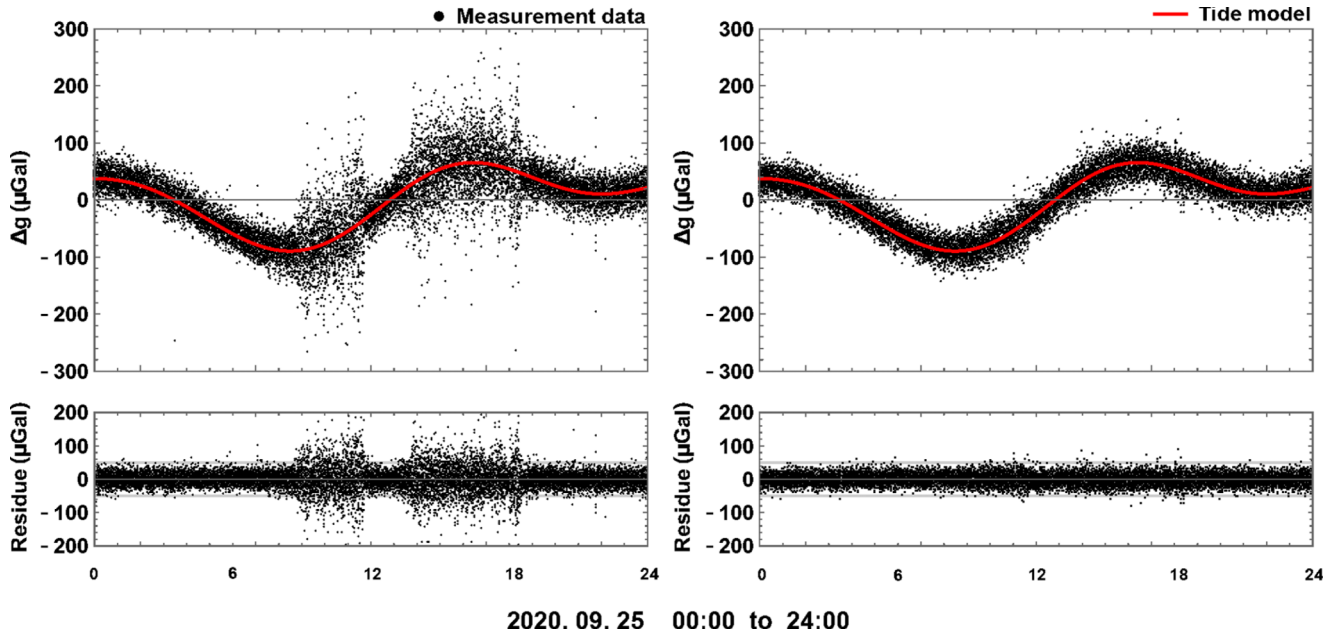

(a)

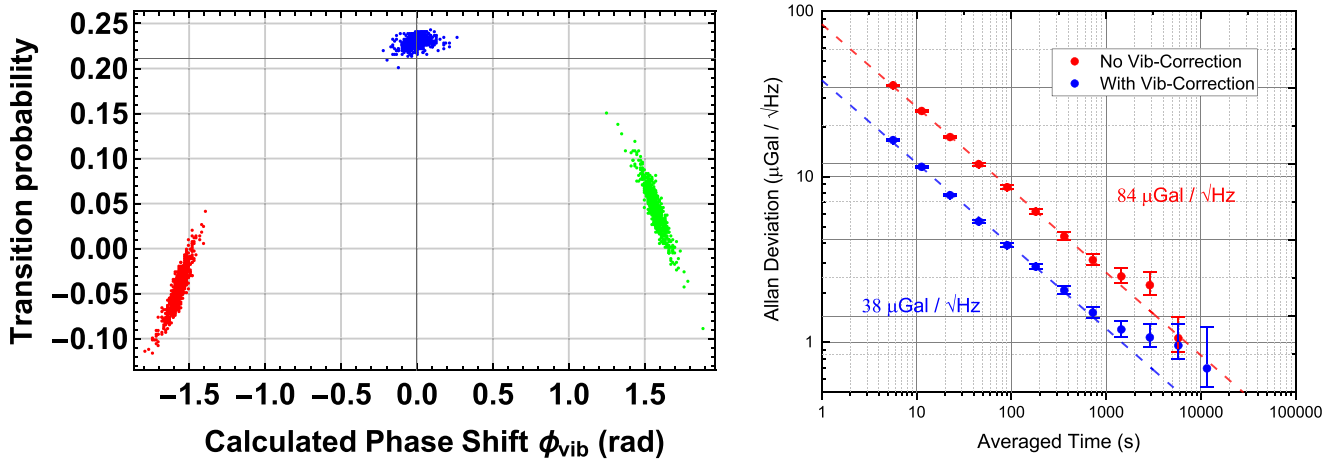

(b) (c)

FIG. 2. (a) The experimental data of the gravitational constant g (the black dot) measured by USTC-AG11 from 12:00 a.m. to 12:00 p.m., on September 25, 2020. The red curve is calculated by TSOFT software based on the earth solid tide model. The original data (left) measured directly by USTC-AG11 is processed by an efficient vibration noise correction (right). (b) The correlation factor between the phase shift caused by vibration noise and the population probability of atoms in $|F = 1\rangle$, 0.92 correlation factor. (c) The standard Allan deviation with vibration correction. The sensitivity has been improved significantly from 84 μGal/$\sqrt{\text{Hz}}$ to 38 μGal/$\sqrt{\text{Hz}}$, which suppressed the overall noise by approximately 80%, and 95% of the vibration noise is effectively suppressed

a half-hour; the red solid curve is the solid tide model calculated by TSOFT. During the measurement of g, there exists an interruption caused by atomic clock off-lock, a one-time interruption caused by a vibration correction method test, and four interruptions caused by a prolonged power outage, marked in Fig. 3. After the first power outage, we went to the TSS to restore the measurement of g. Meanwhile, we added the vibration noise correction method mentioned above. For the remaining three power outages, when the electricity is restored, g measurements start after frequency auto-relock. Figure 3 not only exhibits a good match between the measured data and the tide model, but also illustrates the robustness, long-term stability, and drift-free working ability of USTC-AG11.

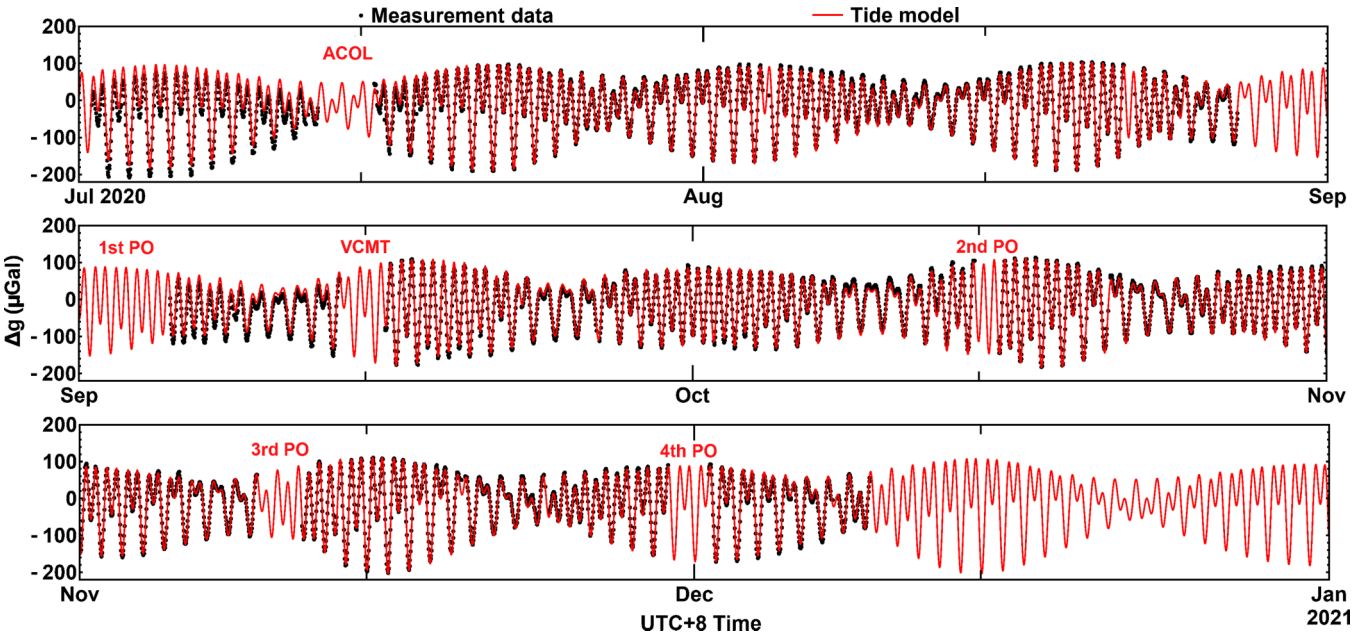

FIG. 3. Continuous stable unattended gravity measurement carried out by USTC-AG11 lasting for more than five months in TSS. The black points are the gravity values measured by USTC-AG11, and each black point is averaged by a half-hour; The red solid line is the solid tide model calculated by TSOFT. There exist one time atomic clock off-lock (ACOL), one time vibration correction method test (VCMT), and four prolonged power outages (PO) during the measurement, marked in the figure, and the other intervals were caused by laser auto-relock.

To characterize the stability of our AG, we randomly pick out two consecutive 48-h periods in each month during the whole measurement (see the Appendix, Fig. 5). The red dots are the residual data obtained by subtracting the theoretical solid tide data from the measured gravity data; each dot is averaged by a half-hour, and the error bar represents the uncertainty of the half-hour measured gravity data, about 1 μGal. Meanwhile, we also calculate the uncertainty between each half-hour measured gravity data, the standard deviation of each consecutive 48-h period is marked in this figure, and the long-term stability of USTC-AG11 is only about 1.3–2.2 μGal. At the same time, we put the red dots into a statistical histogram, and fit it by a Gaussian curve, as shown in Fig. 4, a 1.6 μGal standard deviation obtained with a 0.9907 goodness of fit. This performance is comparable to the best commercial gravimeter FG-5(X). Actually, considering the other environmental variations, such as atmospheric pressure, polar motion, and groundwater subsidence, the performance of our AG would even be better. Even more surprising, after several prolonged power outages caused by local infrastructure, we are still able to restart the measurement of g via remotely accessing the host computer when the electric supply is restored.

IV. CONCLUSION AND PROSPECT

In this paper, we report the performance of a continuous running of a compact atom gravimeter USTC-AG11. It is transported over 2200 km from Shanghai to Yunnan province, and deployed in a seismic station with unattended mode. We realized the continuous gravity measurement over five months from July 1 to December 9, 2020. The robustness and stability of our atom gravimeter are well verified. We established a compact optical package and laser frequency auto-relock module, and the tight fit between them in control timing offers the possibility of long-term gravity measurement. By using the efficient vibration correction method, we obtained

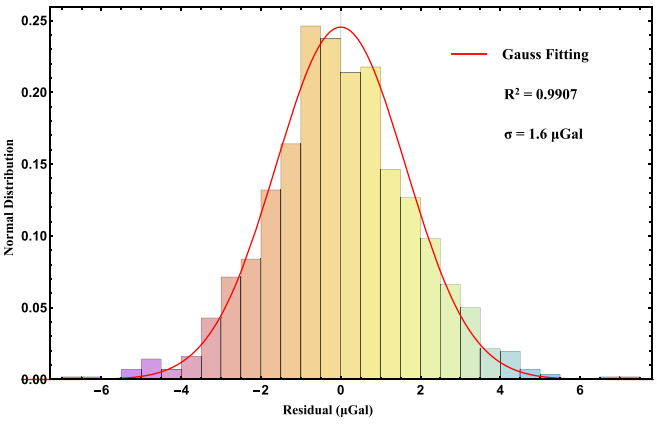

FIG. 4. The normal distribution of the sum of the 48-h residual data for two consecutive periods in each month. The red solid curve is the Gaussian fitting result of the residual data, 1.6 μGal standard deviation with a 0.9907 goodness of fit.

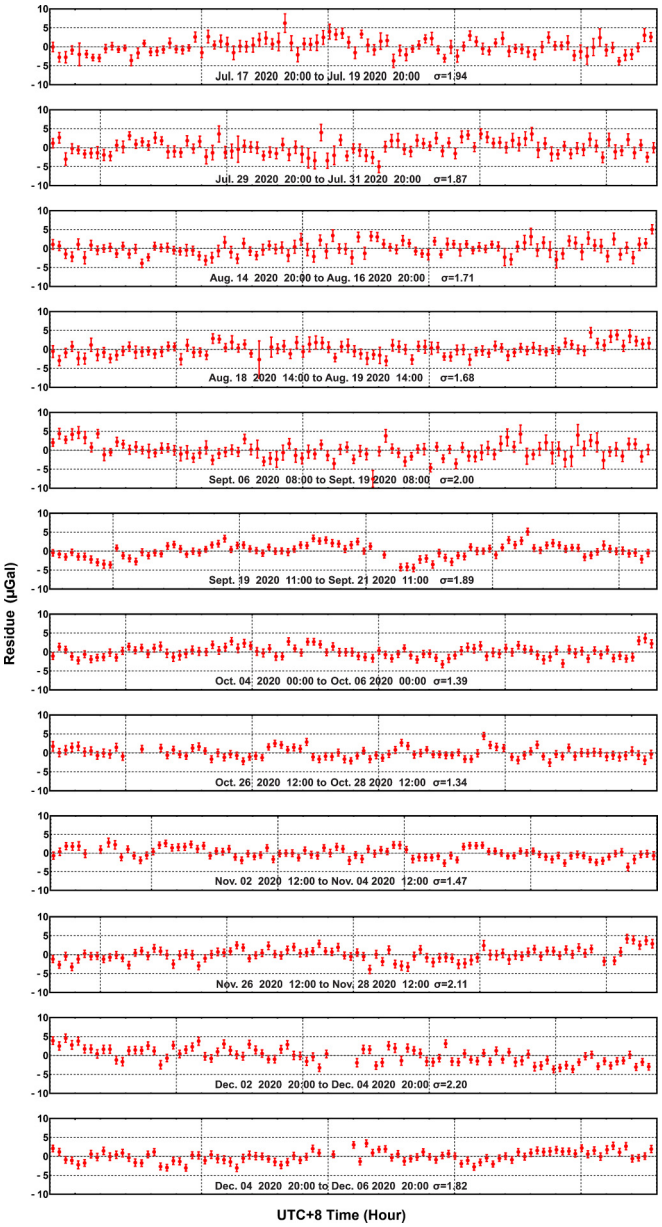

FIG. 5. Typical residual data of two consecutive 48-h periods from July to December.

a good sensitivity of 38 μGal/$\sqrt{\text{Hz}}$, about 1 μGal for 1200 s. We present an excellent performance of this atom gravimeter in a field application, where the measured g values and the tide model data show a good match during the whole measurement, with uncertainty for only about 2 μGal. This performance is comparable to or even better than the best commercial gravimeter FG-5(X). Atom gravimeters are expected to become the priority for long-term precision absolute gravity measurements, and they are likely to play an important role in geophysics, geodesy, or geological disaster observation in the near future.

ACKNOWLEDGMENTS

We thank Xiang-Yang Kong from the Earthquake Administration of Shandong Province, China, for helping us cooperate with the Zhaotong Earthquake Prevention and Disaster Reduction Administration, Yunnan, in the early stage. We thank Chang-Rui Yi for helping us to improve this manuscript. This work was supported by the Innovation Program for Quantum Science and Technology (Grant No. 2021ZD0300601); the Center for Ocean Mega-Science, Chinese Academy of Sciences, the Senior User Project of RV KEXUE (Grant No. KEXUE2020GZ03); the National Natural Science Foundation of China (Grant No. 12025406); Anhui Initiative in Quantum Information Technologies (Grant No. AHY120000); and the Shanghai Municipal Science and Technology Major Project (Grant No. 2019SHZDZX01).

APPENDIX: RESIDUAL PLOT

The Appendix presents the residual data for six months, shows in Fig. 5. Each red point is obtained by a half-hour average, and error bars represent the uncertainty (about 1 μGal) during the half measured gravity data. We also calculate the standard deviations of the residual data, and the uncertainty is 1.3–2.2 μGal.

[1] M. Kasevich and S. Chu, Atomic Interferometry Using Stimulated Raman Transitions, Phys. Rev. Lett. **67**, 181 (1991).

[2] A. Peters, K. Y. Chung, and S. Chu, Measurement of gravitational acceleration by dropping atoms, Nature (London) **400**, 849 (1999).

[3] A. Peters, K. Y. Chung, and S. Chu, High-precision gravity measurements using atom interferometry, Metrologia **38**, 25 (2001).

[4] Z.-K. Hu, B.-L. Sun, X.-C. Duan, M.-K. Zhou, L.-L. Chen, S. Zhan, Q.-Z. Zhang, and J. Luo, Demonstration of an ultrahigh-sensitivity atom-interferometry absolute gravimeter, Phys. Rev. A **88**, 043610 (2013).

[5] C. Freier, M. Hauth, V. Schkolnik, B. Leykauf, M. Schilling, H. Wziontek, H.-G. Scherneck, J. Müller, and A. Peters, Mobile quantum gravity sensor with unprecedented stability, J. Phys.: Conf. Ser. **723**, 012050 (2016).

[6] T. Farah, C. Guerlin, A. Landragin, P. Bouyer, S. Gaffet, F. Pereira Dos Santos, and S. Merlet, Underground operation at best sensitivity of the mobile LNE-SYRTE cold atom gravimeter, Gyroscopy and Navigation **5**, 266 (2014).

[7] V. Ménoret, P. Vermeulen, N. Le Moigne, S. Bonvalot, P. Bouyer, A. Landragin, and B. Desruelle, Gravity measurements below 10^{-9} g with a transportable absolute quantum gravimeter, Sci. Rep. **8**, 12300 (2018).

[8] M. J. Snadden, J. M. McGuirk, P. Bouyer, K. G. Haritos, and M. A. Kasevich, Measurement of the Earth's Gravity Gradient with an Atom Interferometer-Based Gravity Gradiometer, Phys. Rev. Lett. **81**, 971 (1998).

[9] F. Sorrentino, Q. Bodart, L. Cacciapuoti, Y.-H. Lien, M. Prevedelli, G. Rosi, L. Salvi, and G. M. Tino, Sensitivity limits of a Raman atom interferometer as a gravity gradiometer, Phys. Rev. A **89**, 023607 (2014).

[10] X.-C. Duan, M.-K. Zhou, D.-K. Mao, H.-B. Yao, X.-B. Deng, J. Luo, and Z.-K. Hu, Operating an atom-interferometry-based gravity gradiometer by the dual-fringe-locking method, Phys. Rev. A **90**, 023617 (2014).

[11] T. L. Gustavson, P. Bouyer, and M. A. Kasevich, Precision Rotation Measurements with an Atom Interferometer Gyroscope, Phys. Rev. Lett. **78**, 2046 (1997).

[12] B. Canuel, F. Leduc, D. Holleville, A. Gauguet, J. Fils, A. Virdis, A. Clairon, N. Dimarcq, C. J. Bordé, A. Landragin, and P. Bouyer, Six-Axis Inertial Sensor Using Cold-Atom Interferometry, Phys. Rev. Lett. **97**, 010402 (2006).

[13] I. Dutta, D. Savoie, B. Fang, B. Venon, C. L. Garrido Alzar, R. Geiger, and A. Landragin, Continuous Cold-Atom Inertial Sensor with 1 nrad/s Rotation Stability, Phys. Rev. Lett. **116**, 183003 (2016).

[14] Z.-W. Yao, S.-B. Lu, R.-B. Li, K. Wang, L. Cao, J. Wang, and M.-S. Zhan, Continuous dynamic rotation measurements using a compact cold atom gyroscope, Chin. Phys. Lett. **33**, 083701 (2016).

[15] G. Rosi, F. Sorrentino, L. Cacciapuoti, M. Prevedelli, and G. M. Tino, Precision measurement of the Newtonian gravitational constant using cold atoms, Nature (London) **510**, 518 (2014).

[16] R. H. Parker, C. Yu, W. Zhong, B. Estey, and H. Müller, Measurement of the fine-structure constant as a test of the standard model, Science **360**, 191 (2018).

[17] W. Chaibi, R. Geiger, B. Canuel, A. Bertoldi, A. Landragin, and P. Bouyer, Low frequency gravitational wave detection with ground-based atom interferometer arrays, Phys. Rev. D **93**, 021101(R) (2016).

[18] H. Müller, S.-w. Chiow, S. Herrmann, S. Chu, and K.-Y. Chung, Atom-Interferometry Tests of the Isotropy of Post-Newtonian Gravity, Phys. Rev. Lett. **100**, 031101 (2008).

[19] D. Schlippert, J. Hartwig, H. Albers, L. L. Richardson, C. Schubert, A. Roura, W. P. Schleich, W. Ertmer, and E. M. Rasel, Quantum Test of the Universality of Free Fall, Phys. Rev. Lett. **112**, 203002 (2014).

[20] M. G. Tarallo, T. Mazzoni, N. Poli, D. V. Sutyrin, X. Zhang, and G. M. Tino, Test of Einstein Equivalence Principle for 0-Spin and Half-Integer-Spin Atoms: Search for Spin-Gravity Coupling Effects, Phys. Rev. Lett. **113**, 023005 (2014).

[21] X.-C. Duan, X.-B. Deng, M.-K. Zhou, K. Zhang, W.-J. Xu, F. Xiong, Y.-Y. Xu, C.-G. Shao, J. Luo, and Z.-K. Hu, Test of the Universality of Free Fall with Atoms in Different Spin Orientations, Phys. Rev. Lett. **117**, 023001 (2016).

[22] C. Overstreet, P. Asenbaum, T. Kovachy, R. Notermans, J. M. Hogan, and M. A. Kasevich, Effective Inertial Frame in an Atom Interferometric Test of the Equivalence Principle, Phys. Rev. Lett. **120**, 183604 (2018).

[23] P. Gillot, O. Francis, A. Landragin, F. P. D. Santos, and S. Merlet, Stability comparison of two absolute gravimeters: Optical versus atomic interferometers, Metrologia **51**, L15 (2014).

[24] B. Fang, I. Dutta, P. Gillot, D. Savoie, J. Lautier, B. Cheng, C. L. G. Alzar, R. Geiger, S. Merlet, F. P. D. Santos, and A. Landragin, Metrology with atom interferometry: Inertial sensors from laboratory to field applications, J. Phys.: Conf. Ser. **723**, 012049 (2016).

[25] K. Bongs, M. Holynski, J. Vovrosh, P. Bouyer, G. Condon, E. Rasel, C. Schubert, W. P. Schleich, and A. Roura, Taking atom interferometric quantum sensors from the laboratory to real-world applications, Nat. Rev. Phys. **1**, 731 (2019).

[26] S. Wu, J. Feng, C. Li, D. Su, Q. Wang, R. Hu, L. Hu, J. Xu, W. Ji, C. Ullrich, V. Pálinkáš, J. Kostelecký, M. Bilker-Koivula, J. Näränen, S. Merlet, N. L. Moigne, S. Mizushima, O. Francis, I.-M. Choi, M.-S. Kim *et al.*, The results of CCM.G-K2.2017 key comparison, Metrologia **57**, 07002 (2020).

[27] L. Antoni-Micollier, D. Carbone, V. Ménoret, J. Lautier-Gaud, T. King, F. Greco, A. Messina, D. Contrafatto, and B. Desruelle, Detecting volcano-related underground mass changes with a quantum gravimeter, Geophys. Res. Lett. **49**, e2022GL097814 (2022).

[28] X. Wu, Z. Pagel, B. S. Malek, T. H. Nguyen, F. Zi, D. S. Scheirer, and H. Müller, Gravity surveys using a mobile atom interferometer, Sci. Adv. **5**, eaax0800 (2019).

[29] J.-Y. Zhang, W.-J. Xu, S.-D. Sun, Y.-B. Shu, Q. Luo, Y. Cheng, Z.-K. Hu, and M.-K. Zhou, A car-based portable atom gravimeter and its application in field gravity survey, AIP Adv. **11**, 115223 (2021).

[30] H. Wang, K. Wang, Y. Xu, Y. Tang, B. Wu, B. Cheng, L. Wu, Y. Zhou, K. Weng, D. Zhu, P. Chen, K. Zhang, and Q. Lin, A truck-borne system based on cold atom gravimeter for measuring the absolute gravity in the field, Sensors **22**, 6172 (2022).

[31] Y. Bidel, N. Zahzam, C. Blanchard, A. Bonnin, M. Cadoret, A. Bresson, D. Rouxel, and M. F. Lequentrec-Lalancette, Absolute marine gravimetry with matter-wave interferometry, Nat. Commun. **9**, 627 (2018).

[32] Y. Bidel, N. Zahzam, A. Bresson, C. Blanchard, M. Cadoret, A. V. Olesen, and R. Forsberg, Absolute airborne gravimetry with a cold atom sensor, J. Geodesy **94**, 20 (2020).

[33] B. Cheng, Y. Zhou, P.-J. Chen, K.-J. Zhang, D. Zhu, K.-N. Wang, K.-X. Weng, H.-L. Wang, S.-P. Peng, X.-L. Wang, B. Wu, and Q. Lin, Absolute gravity measurement based on atomic gravimeter under mooring state of a ship, Acta Phys. Sin. **70**, 040304 (2021).

[34] H. Che, A. Li, J. Fang, G.-G. Ge, W. Gao, Y. Zhang, C. Liu, J.-N. Xu, L.-B. Chang, C.-F. Huang, W.-B. Gong, D.-Y. Li, X. Chen, and F.-J. Qin, Ship-borne dynamic absolute gravity measurement based on cold atom gravimeter, Acta Phys. Sin. **71**, 113701 (2022).

[35] J.-B. Long, S.-J. Yang, S. Chen, and J.-W. Pan, Magnetic-enhanced modulation transfer spectroscopy and laser locking for ^{87}Rb repump transition, Opt. Express **26**, 27773 (2018).

[36] J. Le Gouët, T. E. Mehlstäubler, J. Kim, S. Merlet, A. Clairon, A. Landragin, and F. Pereira Dos Santos, Limits to the sensitivity of a low noise compact atomic gravimeter, Appl. Phys. B **92**, 133 (2008).

[37] B. Barrett, L. Antoni-Micollier, L. Chichet, B. Battelier, P.-A. Gominet, A. Bertoldi, P. Bouyer, and A. Landragin, Correlative methods for dual-species quantum tests of the weak equivalence principle, New J. Phys. **17**, 085010 (2015).

[38] S. Merlet, J. L. Gouët, Q. Bodart, A. Clairon, A. Landragin, F. P. D. Santos, and P. Rouchon, Operating an atom interferometer beyond its linear range, Metrologia **46**, 87 (2009).